J Seismol (2009) 13:141–160
DOI 10.1007/s10950-008-9132-0

ORIGINAL ARTICLE

Attenuation of coda waves in the Northeastern Region of India

Devajit Hazarika · Saurabh Baruah · Naba Kumar Gogoi

Received: 27 December 2006 / Accepted: 4 August 2008 / Published online: 5 September 2008

Abstract Coda wave attenuation quality factor Qc is estimated in the northeastern region of India using 45 local earthquakes recorded by regional seismic network. The quality factor Qc was estimated using the single backscattering model modified by Sato (J Phys Earth 25:27–41, 1977), in the frequency range 1–18 Hz. The attenuation and frequency dependence for different paths and the correlation of the results with geotectonics of the region are described in this paper. A total of 3,890 Qc measurements covering 187 varying paths are made for different lapse time window of 20, 30, 40, 50, 60, 70, 80, and 90 s in coda wave. The magnitudes of the analyzed events range from 1.2 to 3.9 and focal depths range between 7 and 38 km. The source–receiver distances of the selected events range between 16 and 270 km. For 30-s duration, the mean values of the estimated Qc vary from 50 ± 12 (at 1 Hz) to 2,078 ± 211(at 18 Hz) for the Arunachal Himalaya, 49 ± 14 (at 1 Hz) to 2,466 ± 197 (at 18 Hz) for the Indo-Burman, and 45 ± 13 (at 1 Hz) to 2,069 ± 198 (at 18 Hz) for Shillong group of earthquakes. It is observed that Qc increases with frequency portraying an average attenuation relation $Qc = 52.315 \pm 1.07\, f^{(1.32 \pm 0.036)}$ for the region. Moreover, the pattern of Qc^{-1} with frequency is analogous to the estimates obtained in other tectonic areas in the world, except with the observation that the Qc^{-1} is much higher at 1 Hz for the northeastern region. The Qc^{-1} is about $10^{-1.8}$ at 1 Hz and decreases to about $10^{-3.6}$ at 18 Hz indicating clear frequency dependence. Pertaining to the spatial distribution of Qc values, Mikir Hills and western part of Shillong Plateau are characterized by lower attenuation.

Keywords Qc · Coda waves · Single backscattering · Frequency dependence · Northeastern India

D. Hazarika · S. Baruah (✉)
Geoscience Division,
Regional Research Laboratory (CSIR),
Jorhat 785 006, Assam, India
e-mail: saurabhb_23@yahoo.com

N. K. Gogoi
Seismological Observatory,
National Geophysical Research Institute (CSIR)
Uppal Road, Hyderabad 500 007, India

1 Introduction

Northeast region (NER) of India, bounded by latitude (22–30° N) and longitude (89–98° E), is seismically one of the most active zones in the world where 16 large ($M \geq 7.0$) and two great earthquakes of June 12, 1897 ($M \geq 8.5$; Oldham 1899) and August 15, 1950 ($M = 8.7$; Poddar 1950; Richter 1958) occurred during the last hundred

years. These two great earthquakes have caused extensive destruction in the region killing a total of 3,042 lives and a total loss of $30 million (Tillottson 1953). Consequently, the NER India lies in the seismic zone V of India (BMTPC 2003). The zone V is the maximum rating of zone in the National Seismicity Zoning Map of India. Mainly three major stress fields govern the geodynamics of NER, India. There are several tectonic faults and lineaments (Nandy 2001). The active seismotectonics of the region has been the subject of several studies (e.g., Tapponier et al. 1982; Le Dain et al. 1984; Mitchel 1986; Gupta and Singh 1986; Chen and Molnar 1990; Kayal 1996; Saikia and Somerville 1998). Several hundred of earthquakes ($M > 4.0$) are recorded during the past decade in the region. In view of this high seismic activity and with an intension to upgrade the improved detection capabilities, Regional Research Laboratory, Jorhat (RRL-J) in collaboration with National Geophysical Research Institute, Hyderabad (NGRI-H) established progressively 14 vertical component and two three-component seismic stations equipped with short-period instrumentation in the year 1982. These stations are now upgraded to broadband digital stations with global positioning system (GPS) timing since 2001. The hypocentral parameters are regularly published in the form of seismic bulletins. The complex geotectonic setup of the NER needs better understanding of the measure of elastic wave attenuation and scattering in the crust. This region is not represented by any proper attenuation relationship of the seismic waves based on digital seismic database. The variation of coda Q was reported by Baruah (2001) using four earthquakes recorded by the Digital Telemetered Seismic Network of the RRL-J, a dependence of Qc on frequency varying from 86 at 1.5 Hz to 960 at 12 Hz under the relationship $Qc = 121\ f^{0.86}$ was observed for a lapse time window of 30-s duration in coda wave. Based on strong motion records of a single earthquake of 6 August, 1988 originated in Indo-Burmese subduction zone (Lat = 25.14° N, Long = 95.12° E, mb = 6.8 and h = 91 km), Gupta and Kumar (2002) suggested a frequency-dependent Qc relationship, $Qc = (86 \pm 4.04)\ f^{(1.01 \pm 0.026)}$ for the Shillong–Mikir plateau and North of Halflong–Disang thrust. Not much study on the attenuation property of the crust is made in the region. In the present study, we have used the broadband seismic waveform data to establish a suitable attenuation relation in NER India. One of the promising means to study seismic wave attenuation in the crust and lithosphere is the analysis of the coda wave of local earthquakes (Aki 1969; Aki and Chouet 1975; Sato 1977). Coda waves, the later part of the seismogram, are assumed to consist of backscattered S wave, which represent the heterogeneities in the propagating media and provide the information about the average attenuation properties of the medium. The rate of decay of coda wave amplitude gives an idea about the attenuation. Aki (1969) and Sato (1977) proposed that the rate of decay could be quantified by a quality factor Qc or coda Q, characterized by seismic wave scattering, with higher values of Qc representing slower decay. Several authors (e.g., Aki and Chouet 1975; Sato 1977; Rautian and Khalturin 1978; Herrmann 1980; Roecker et al. 1982; Ibanez et al. 1990; Herak 1991; Novelo-Casanova and Lee 1991; Woodgold 1992; Gupta et al. 1998; Giampiccolo et al. 2004; Biescas et al. 2007) observed that the use of coda wave is the easiest way to estimate the attenuation, backscattering, and source spectrum. Generally, the attraction of using coda is the isolation of scattered energy from the other phases. Qc estimates the attenuation per travel distance on the basis of spatially uniform distribution of coda-energy at a long lapse time.

In this study, a single backscattering model proposed by Aki and Chouet (1975) and modified by Sato (1977) has been used to estimate quality factor Qc for three tectonic blocks in NER, India, namely Eastern Himalaya and suture zone, Shillong Plateau and Mikir Hills, and Indo-Burmese region. The results of this study are highlighted here.

2 Tectonic setup and seismicity

The area of present study, delimited by latitude 22° to 30° N and longitude 89° to 98° E, covers the NER, India and the adjoining areas (Fig. 1).

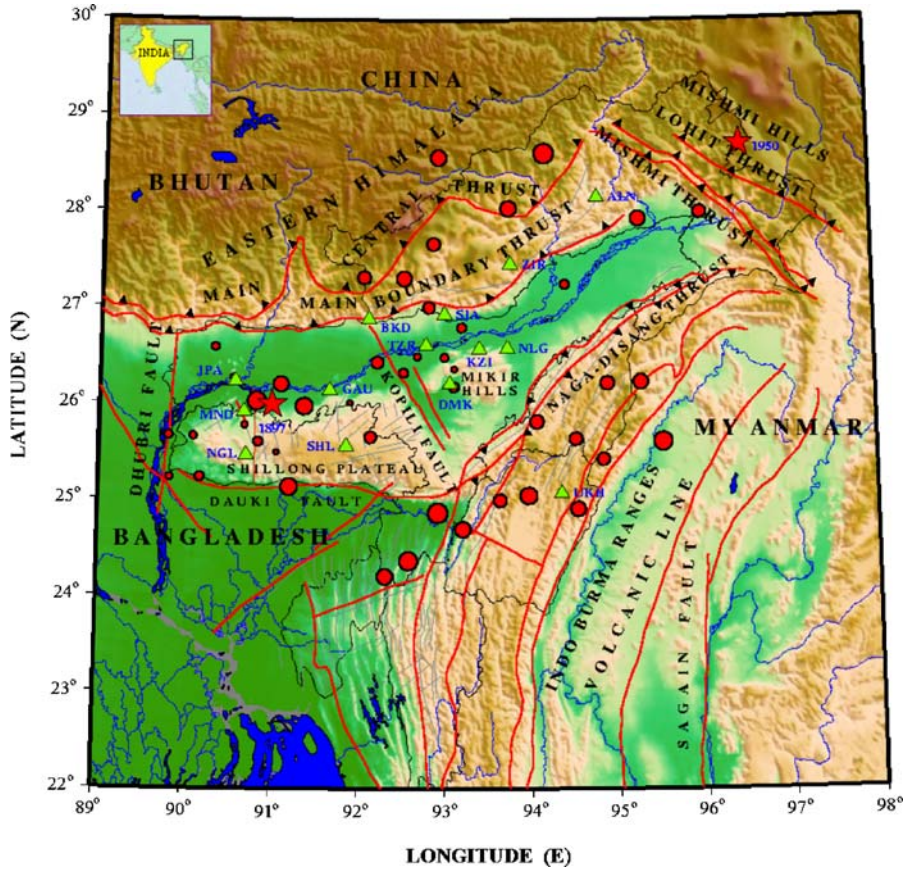

Fig. 1 Tectonic map of North Eastern Region of India showing epicentral distribution of the events used in this study and the RRL-J–NGRI-H broadband recording stations supplemented by stations operated by Manipur University and Gauhati University

The region under study can be divided into the following tectonic domains (Nandy 2001):

1. The eastern Himalaya collision belt to the north, which includes the trans-Himalayan Tethyan zone and the Andean type granodiorite margin comprising the main boundary thrust (MBT) and main central thrust (MCT). The Eastern syntaxis zone where the Himalayan arc and the Burmese arc meets the Mishimi block. This zone is folded and thrusted by the Lohit and Mishimi thrusts (MT). This zone was the source area for the 1950 great earthquake.
2. The Indo-Burma subduction zone to the east where the Indian lithosphere is believed to be subducting below Indo-Burma ranges. (Satyabala 1998)
3. The Shillong Plateau, the Mikir Hills, and the Assam valley jawed between the Himalayan arc and Burma arc (Mazumder 1976; Curray et al. 1982). The major tectonic features are the Dauki fault and Kopili fault. The E–W trending Dauki fault separates the Shillong Plateau to the north and the Bengal basin to the south, and the NW trending Kopili fault separates the Shillong Plateau and the Mikir Hills (Fig. 1).

Among the other tectonic features, the N–S trending Dhubri fault and the Brahmaputra lineament are prominent. Dhubri fault demarcates the western margin of the Shillong Plateau.

The seismic activity in NER is mostly associated with these major tectonic elements. Several authors (e.g., Fitch 1970; Chen and Molnar 1990; Nandy and Das Gupta 1991; Kayal 1996; Sitaram et al. 2001) discussed the seismicity and seismotectonics of the region. The major fault systems, i.e., MBT, MCT in the north, and MT towards northeast, show activity with shallow earthquakes. There are numbers of seismic events

concentrating near Tezpur (south of the MBT) and Kaziranga (in Mikir Hills) and extending along the Brahmaputra lineament. The upper Brahmaputra (Assam) valley seems to be broadly aseismic (Khattri 1987).

In the Indo-Burma tectogene, based on CMT catalog data, Ravikumar et al. (1996) suggested right lateral strike-slip faulting mostly in the upper part of the zone and thrust faulting below 90-km depth. Satyabala (1998), based on the stress field study, argued that there is an active subduction of the Indian plate below the Indo-Burma ranges.

Shillong plateau covering Chedrang fault, Dhubri fault, and Dauki fault system shows significant activity; the trend of P-axis of the focal mechanism solutions has been dominantly NNW. This indicates that contemporary tectonics of this tectonic domain have been governed by NNW-directed stress field (Baruah et al. 1997). The seismic activities in the Shillong Plateau are found notably high at a depth range of 10–20 km with an average seismogenic zone up to 30 km (Baruah 2004). Mostly thrust faulting earthquakes are predominant in the Shillong Plateau. The plateau had been the source area for the 1897 great Assam earthquake. Pop-up tectonics is advocated for the plateau seismicity (Bilham and England 2001).

3 Data source

In this study, we selected 45 earthquakes (see Table 1) recorded by regional seismic network (RRL-J and NGRI-H) during 2000–2003. These events are recorded with higher signal-to-noise ratio and having clear coda waves. One hundred eighty-seven seismograms were used for the selected 45 events. The epicentral distribution of the selected earthquakes is shown in Fig. 1.

The precision of hypocenter determination depends not only on the distribution of the recording stations but also on velocity structure between source and station, particularly in area where lateral heterogeneities are extreme (Okada et al. 1970). The epicenters are determined using the HYPOCENTER location program of Lienert et al. (1986) based on the crustal velocity model of Gupta et al. (1984). To the present database, the uncertainties involved in the estimates of epicenters and origin times are of the order 0–2 km and 0–0.5 s, respectively. The uncertainties involved in the estimates of focal depths are 0–1 km for 85% and 1–2 km for 15% of total number of earthquakes located. We believe that the depth control is reasonably good. Besides the RRL-J–NGRI-H network data, the arrival time data also used are reported by the seismic stations maintained by the India Meteorological Department at SHL, Gauhati University, Manipur University, and Mizoram University. This provided better azimuthal control for the determination of hypocentral parameters. Incidentally, some of these digital seismic stations are also equipped with broadband seismometers as depicted in Table 2. Waveforms obtained from these stations are also used in this study. GPS time synchronization was maintained with the records. The stations are operated both in continuous and event-trigger mode and recorded at a rate of 100 samples per second. To avoid aliasing effects, low pass filters with corner frequencies of 50 Hz were applied. The recorded seismograms have been corrected by using an instrument response based on the electrodynamic constant, critical damping, natural frequency of seismometer, and bit weight of unit gain of each recording unit for all stations. Figure 2 shows an example for the station Mendipather (MND) in East Garo Hills, Meghalaya, that contains a typical estimate of (a) frequency response to the ground velocity with known pole-zero distribution and (b) the plot of the system noise power as noncoherent power for vertical (Z = red) and horizontal sensors (N = green and E = blue) up to 10-s period band. The power spectral estimates have been corrected for the system response and gain representing the sensor input. The station MND is instrumental in the low-noise model (LNM; Peterson 1993); however, the highest power levels (red, green, and blue) are not significantly higher (<26%) than the LNM. The three lines approach the LNM indicating that the station minimum reflects actual ambient noise conditions across the whole spectrum.

The source–receiver distances of the selected event range from 16 to 270 km. Duration magnitude (M_D) of the events are estimated in the

Table 1 Hypocentral parameters of the events used in this study

Sl. no.	Date	Origin time			Location		Focal depth	Magnitude
		Hr.	Mn.	Sec.	Lat.°N	Long.°E	(km)	(M_DA)
1	20000813	12	16	20.53	27.99	96.00	21	3.2
2	20011118	18	15	47.85	25.82	94.07	20	3.3
3	20011118	19	37	26.30	26.18	93.11	36	2.8
4	20011118	20	18	44.89	27.93	95.27	32	3.4
5	20011118	22	32	48.57	26.33	92.52	35	2.7
6	20011119	12	16	43.43	26.03	90.82	27	3.8
7	20011120	19	06	50.38	25.00	93.64	28	3.2
8	20011120	21	35	04.12	26.80	93.20	10	2.7
9	20011121	04	51	50.85	26.22	94.89	21	3.3
10	20011121	11	52	28.64	27.01	92.82	24	3.0
11	20011121	12	31	44.47	26.50	92.68	37	2.4
12	20011122	11	53	55.98	26.37	93.11	10	2.1
13	20011122	12	48	24.73	24.70	93.21	20	3.5
14	20011123	13	11	36.25	26.49	93.00	30	2.5
15	20011123	15	41	19.19	27.31	92.53	22	3.4
16	20011123	18	58	02.67	24.91	94.54	30	3.4
17	20011124	22	10	42.65	28.04	93.75	20	3.5
18	20011125	12	53	39.36	26.44	92.22	38	3.1
19	20011125	18	03	55.08	25.98	91.37	12	3.6
20	20011126	22	55	01.04	25.64	94.52	28	3.2
21	20011127	01	30	49.26	25.43	94.84	35	3.1
22	20011127	11	15	43.86	25.05	93.97	32	3.6
23	20011127	13	47	05.13	28.61	94.17	30	3.6
24	20011127	13	47	07.97	28.57	92.93	7	3.5
25	20011128	01	34	01.67	26.23	95.28	38	3.4
26	20011129	12	19	57.68	25.66	92.14	17	3.0
27	20011129	19	42	27.16	24.21	92.31	20	3.5
28	20011129	21	12	11.01	27.32	92.06	13	3.2
29	20011207	16	16	27.80	24.37	92.58	20	3.8
30	20011208	22	08	57.99	26.21	91.10	12	3.4
31	20011211	18	22	09.19	27.67	92.87	22	3.2
32	20011211	19	09	49.82	24.87	92.92	24	3.9
33	20011212	23	06	08.21	25.14	91.20	14	3.6
34	20011214	21	42	42.99	25.61	95.53	17	3.8
35	20011216	22	25	27.82	27.25	94.40	21	2.7
36	20030820	11	52	26.00	25.67	89.80	11	2.5
37	20030820	19	28	22.20	25.50	91.05	9	1.8
38	20030823	00	57	47.20	25.61	90.84	14	2.7
39	20030823	11	35	33.70	26.28	90.54	9	2.0
40	20030929	18	45	15.08	26.02	91.90	13	1.5
41	20030930	12	36	40.30	25.66	90.09	12	2.1
42	20030930	18	14	18.24	25.24	90.17	20	2.7
43	20031001	18	51	24.20	26.59	90.33	23	2.5
44	20031004	15	18	15.60	25.23	89.82	22	2.3
45	20031005	21	02	55.00	25.78	90.68	16	1.2

range 1.2–3.9 and the depth 7–38 km. The events are selected so that these are recorded locally by at least three stations in the respective tectonic block, supplemented by two more stations in the neighboring tectonic block so that there is conformity of source–receiver path among three selected tectonic blocks. Figure 3 presents the corresponding epicenter–station trajectories.

Table 2 Parameters of seismological stations (e.g., name, code, and their location)

SL. no.	Station name	Station code	Latitude (°N)	Longitude (°E)
1	Along	ALN	28.15	94.79
2	Bhairabkunda	BKD	26.89	92.12
3	Dokmok	DMK	26.22	93.06
4	Gauhati	GAU	26.15	91.67
5	Jogighopa	JPA	26.24	90.57
6	Kaziranga	KZI	26.58	93.41
7	Mendipather	MND	25.92	90.68
8	Nangalbibra	NGL	25.47	90.70
9	Numaligarh	NLG	26.58	93.73
10	Shillong	SHL	25.57	91.86
11	Seijusa	SJA	26.94	93.00
12	Tezpur	TZR	26.62	92.78
13	Ukhrul	UKH	25.08	94.35
14	Ziro	ZIR	27.54	93.80

4 Data analysis

Two backscattering models explain the coda wave amplitude on a seismogram. The first is the single scattering model, which assumes that the scattering wave field is weak and does not produce secondary scattering when it encounters another scatterer (Aki and Chouet 1975). The second model is the multiple scattering model (Gao et al. 1983), which assumes secondary scattering and consider the seismic energy transfer as a diffusion process. In this study, the attenuation of coda waves is measured as a function of frequency using the data from local earthquakes with the help of single scattering model. We assumed that the source and the receiver are located at the same point in an infinite medium. This is a valid assumption for coda waves, which arrive at the receiver long after the passage of the primary P, and S waves after twice the S-wave lapse time, having a common envelope shape at most stations near the epicenter (Rautian and Khalturin 1978).

In order to establish a suitable attenuation relation, the entire NER has been segregated into three tectonic groups as per distribution of epicentral location in conformity with tectonic features in the region. The events located on the Eastern Himalaya and suture zone are referred to as the Arunachal (AR) group. The central group consists of events located in Shillong Plateau and Mikir Hills designated as SHL (Shillong) group and the events located along Naga–Disang thrust and Indo-Myanmar zone are included in Indo-Burmese region (IBR) group. The attenuation of coda waves is measured as a function of frequency to measure the total scattering coefficient and coda attenuation, which characterize coda excitation and coda amplitude decay. The studies are conducted at short and intermediate epicentral distance of 16–270 km. The decay of coda wave amplitudes is analyzed at different lapse time windows. Finally, attenuation relationship for each tectonic block is deduced leading to an average attenuation relationship for the NER. Figure 4 shows an example of seismogram (event no. 14 in Table 1) from a local earthquake recorded by the Dokmok (DMK) station.

The time dependence of root mean square (RMS) coda wave amplitude, A(ω, t), on a band-pass-filtered seismogram can be written as

$$A(\omega,\ t) = C(\omega)\,.\,t^{-1}\exp(-\omega t/2Q_c) \qquad (1)$$

where Q_c is the attenuation quality factor as a function of frequency, t^{-1} is a correction factor for the geometrical spreading, and $C(\omega)$ takes into account these terms of source and site amplification.

Sato (1977) developed the model where RMS coda wave amplitude at lapse time t may be written as

$$A(r,\ \omega,\ t) = C(\omega)\,[K(r,\ x)]\ \exp(-\omega t/2Q_c) \qquad (2)$$

where, t/ts $= x$ (ts is the travel time of S wave). $K(r\ ,\ x)$ is a function of station–source distance, and r defined as

$$K(r,\ x) = 1/r \times 1/x \times \ln\left[(x+1)/(x-1)\right] \qquad (3)$$

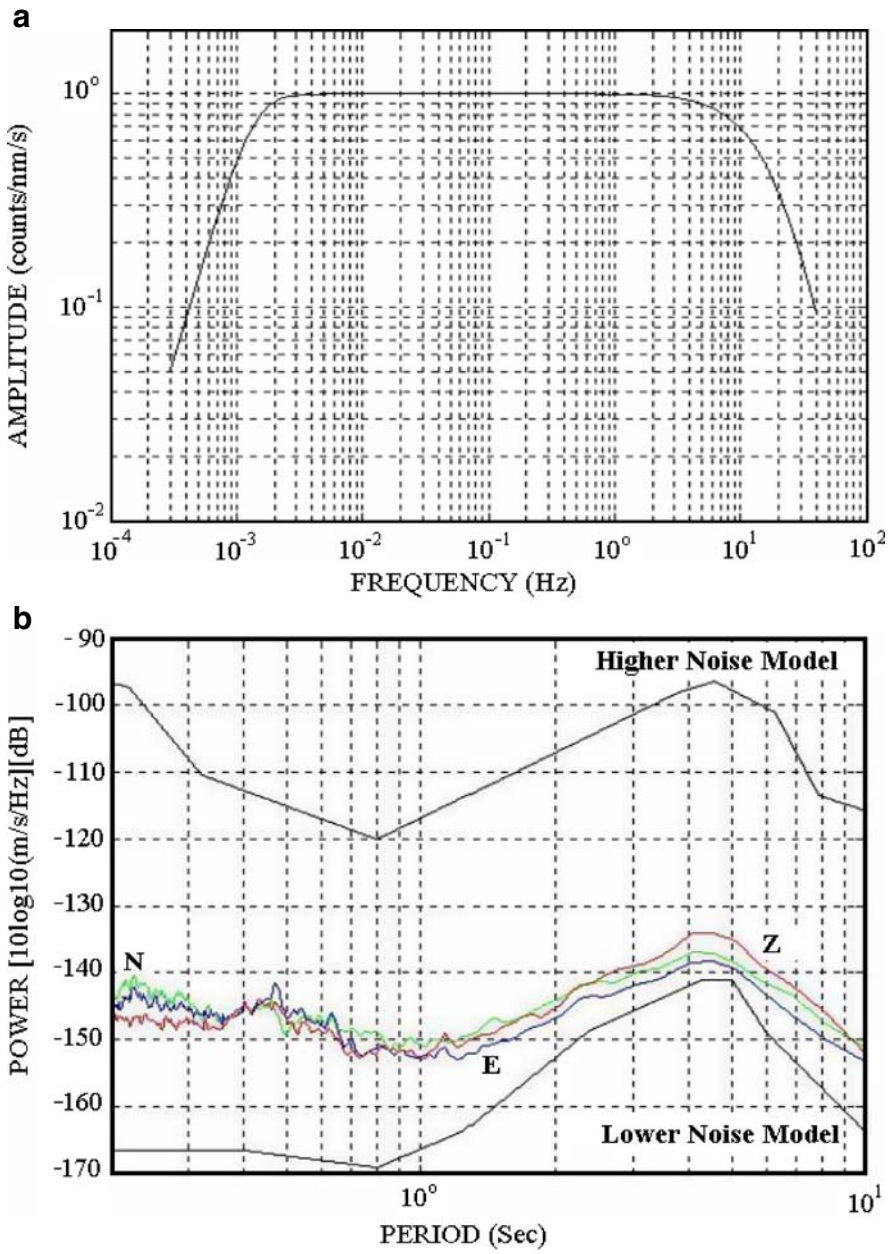

Fig. 2 The figures given above are an example for station MND-Mendipather, East Garo Hills, Meghalaya contain a typical estimate of **a** frequency response to the ground velocity with known pole-zero distribution and **b** the system noise power plotted as noncoherent power for vertical (Z = red) and horizontal sensors (N = green and E = blue)

By taking the natural logarithms of Eq. 2 and rearranging terms, we obtain the following equation:

$$\ln\left[A(r,\omega,t)/K(r,\ x)\right]=\ln\left[C(\omega)\right]-(\omega t/2Q_c) \quad (4)$$

For narrow band-pass-filtered seismograms, $C(\omega)$ is constant. Therefore, by using a linear regression of terms on the left side of Eq. 4 vs t, Q_c can be determined from the slope of the fit, which is equal to $-\omega/2Q_c$.

In order to study the frequency and lapse time dependence of Qc, we use following scheme to analyze the data

(a) The seismograms are filtered for narrow frequency bands centered at fc = 1, 1.5, 2, 3, 4, 6, 8, 12, 16, and 18 Hz, respectively, using eight-

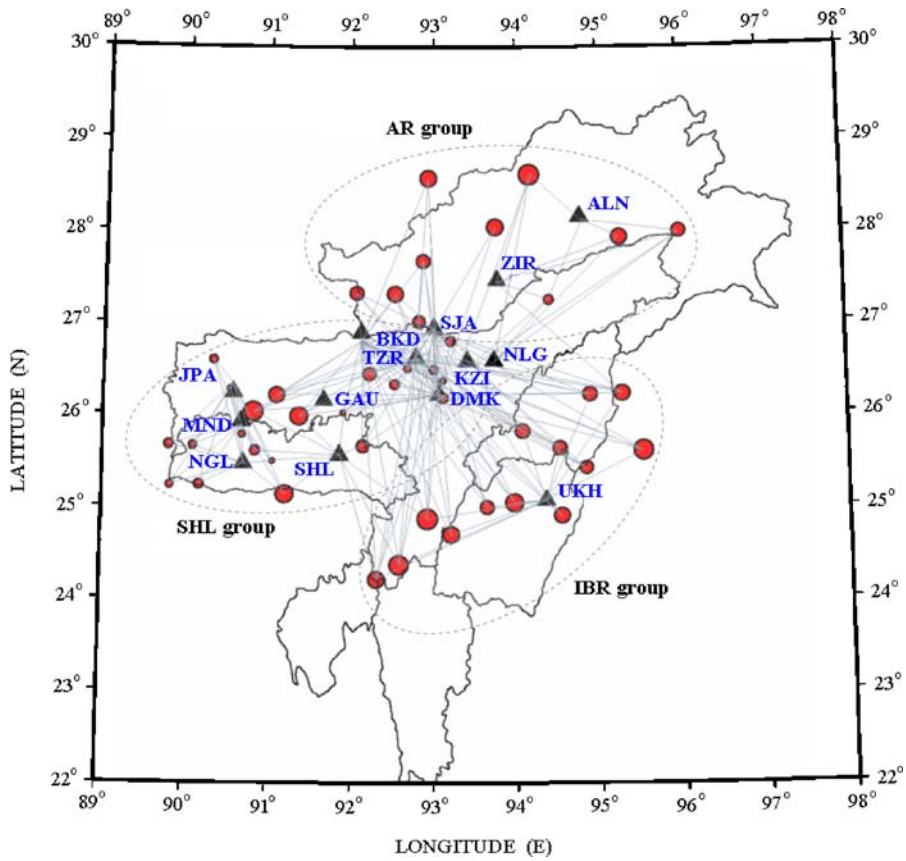

Fig. 3 Map showing epicenter–station trajectories. The area covered by epicenter–station paths provides representative average coda-Q values for the NER, India under study. *Dashed line* demarcates events from each tectonic group

pole Butterworth band pass filter (Stearns and David 1988). The ten frequency bands (bandwidth 0.67 fc, where fc is the central frequency) with filter parameters are given in Table 3.

(b) The beginning of coda amplitude starts at 2 *ts*, where *ts* is the travel time of S wave measured from the origin time of the earthquake (Rautian and Khalturin 1978).

(c) For Qc estimation, a moving window (W) of fm × (SPS) second is used to estimate the RMS average of the filtered coda amplitude which slides in steps of 0.5 × fm × (SPS) second. Here, fm stands for mean free number of points within the time window and "SPS" stands for samples per second. The filtered coda amplitudes are smoothed by determining RMS amplitude for sliding window of 1.28, 2.56, and 5.12 s in steps of half of the time window, i.e., 0.64, 1.28, and 2.56 s, respectively, for lapse time range. The RMS amplitude values are assigned to the center point of corresponding window.

(d) Once the set of $A(r, \omega, t) / K(r, x)$ and the coda intervals are obtained beginning at 2 *ts*, Qc could be easily estimated from the slope of the linear fit of Eq. 4, $\ln [A(r, \omega,t)/K(r, x)]$ vs. t, the lapse time.

(e) In the next step, the lapse time dependence of Qc is observed by increasing the coda duration step by step, measured from origin time. Each seismogram falling in the lapse time range of 20–90 s is analyzed starting at 2 *ts*.

Coda Q values were determined using waveform data from all the events listed in Table 1. In order to provide an average picture of each earthquake group, we averaged all the Qc values determined at each station and for each frequency. The average Qc values were calculated using STDEV algorithm.

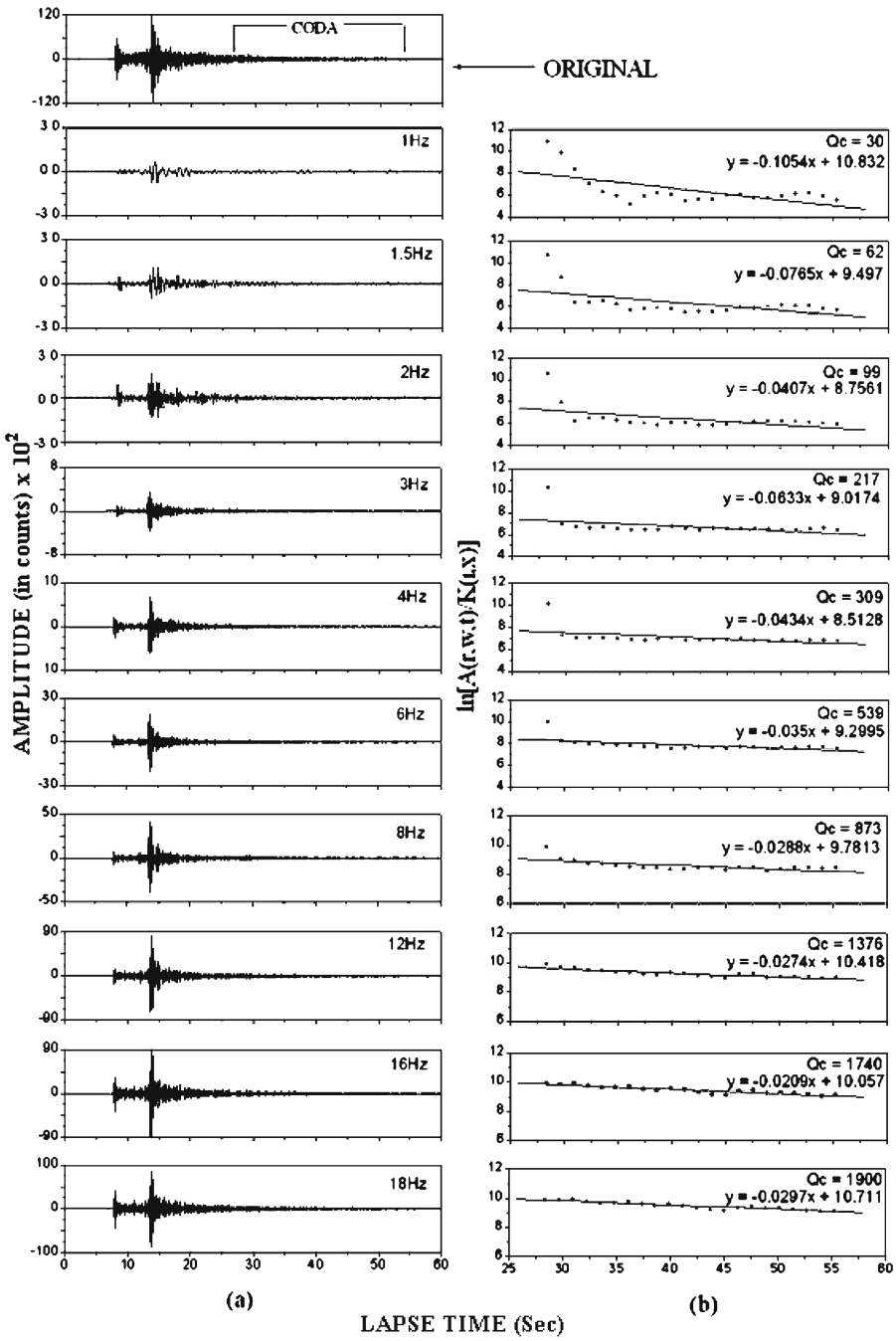

Fig. 4 **a** An example of original and band-pass-filtered seismograms from station DMK recorded on 23 November 2001 (event no. 14 in Table 1). The coda wave portion of 30-s window length indicated by *arrows*. **b** Plot of logarithmic of geometrical spreading corrected and smoothed coda amplitudes as a function of lapse time for the window selected in **a**

There is a clear effect of increase of lapse time window on Qc values. As the lapse time window become longer after 2 *ts*, the Qc values exhibit two distinguished uniqueness: the scatter reduces noticeably and the value of Qc increases. The higher the lapse time window, the higher the Qc values. Measuring Qc from different lapse time windows can cause its value to change significantly. The events with lower magnitude possess smaller duration while a larger magnitude event will produce a longer recording. Hence, for lower magnitude event, Qc can be measured for less numbers of lapse time window than that of larger magnitude event. Variation in amplitude in a lapse

Table 3 Parameters of band pass filters showing central frequencies with respective low and high cutoff frequencies

Low cutoff (Hz)	Central frequency (Hz)	High cutoff (Hz)
0.67	1.0	1.33
1.00	1.5	2.00
1.33	2.0	2.67
2.00	3.0	4.00
2.67	4.0	5.33
4.00	6.0	8.00
5.33	8.0	10.67
8.00	12.0	16.00
10.67	16.0	21.33
12.00	18.0	24.00

time window contributes significantly to the estimation of Qc values with an event of higher signal-to-noise ratio. Averaging is done separately on filtered waveform at different frequency bands for varying lapse time window. While doing so, it is observed that the envelope of coda wave is perfectly smoothed for 5.12- and 2.56-s sliding window in lower- and higher-frequency bands, respectively. Sliding window of 1.28 s shows scatter in RMS amplitudes of the coda envelope. That is why finally we have sliding window of 5.12 s (for 1 and 1.5 Hz) and 2.56 s (for 3, 4, 6, 8, 12, 16, and 18 Hz) for obtaining the average values. The RMS values obtained by this approach constitute a smoother envelope of the coda, which is multiplied by the lapse time (t) for applying geometrical spreading correction. Figure 4a shows all the filtered seismograms with the smoothed logarithmic amplitude of the coda part of the seismogram as shown in Fig. 4b. In this example, respective Qc values were calculated from the slope over the whole lapse time range.

5 Results

To systematically study the attenuation of coda wave, a total of 3,890 Qc values are estimated from

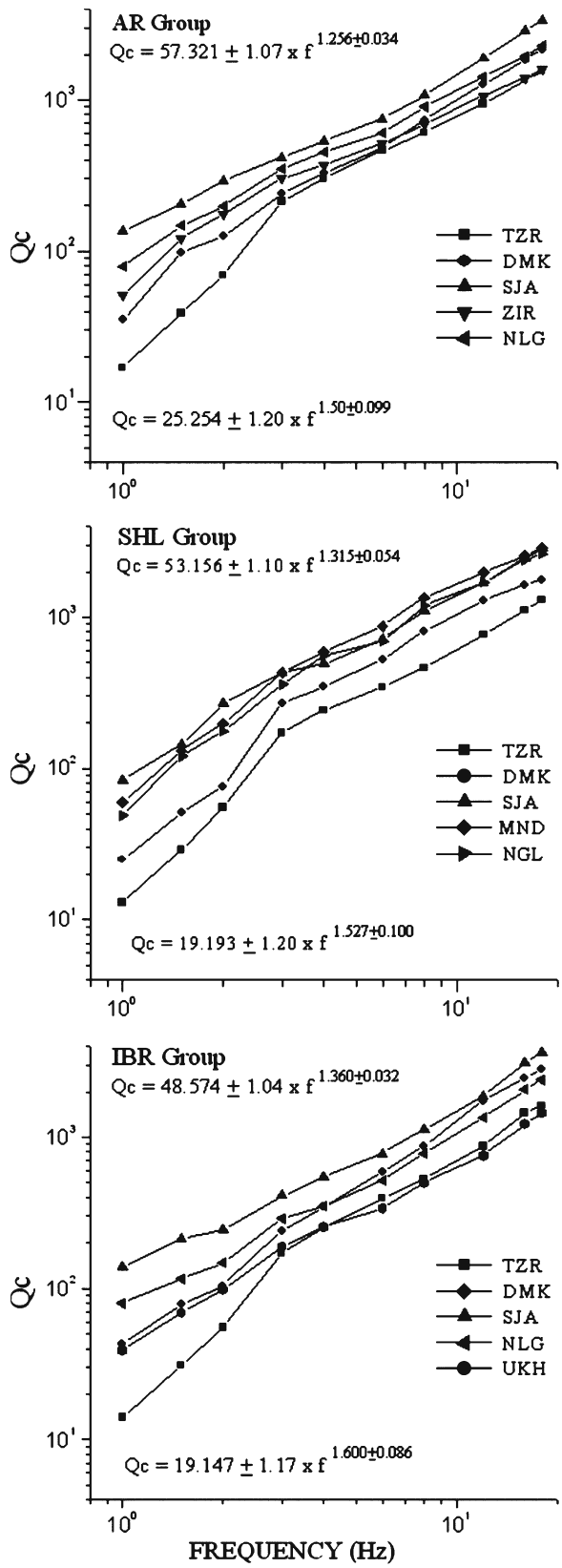

Fig. 5 Figure showing the estimated average coda Qc values plotted as a function of frequency for AR, SHL, and IBR regions using 30-s coda window length. *Different symbols* are used to represent Qc values estimated at different stations. The average attenuation relation for each group is indicated at the *top* while attenuation relation separately obtained for TZR station is indicated at the bottom of each plot

the analysis of 20–90-s lapse time windows in the frequency range 1–18 Hz, covering 187 varying station–source paths (Fig. 3).

5.1 Attenuation characterization

The first one takes all the results obtained from analysis of 30-s lapse time window to portray the attenuation characteristics of each tectonic block, i.e., AR, SHL, and IBR, respectively. Finally, we consider Qc estimates from 20-, 40-, 50-, 60-, 70-, 80-, and 90-s lapse time windows. Exclusively, a total of 930 Qc measurements are made from the analysis of 30-s window. In the analysis, a fixed window is used for all the events to obtain stable measurements, for example, 25–55 s in case of 30-s window (Fig. 4). As mentioned earlier, all Qc values are averaged at each central frequency for AR, SHL, and IBR group of events (see Table 4). The average value of Qc for 30 s varies from 50 ± 12 (at 1 Hz) to 2,078 ± 211 (at 18 Hz) for the AR group, 49 ± 14(at 1 Hz) to 2,466 ± 197(at 18 Hz) for the IBR group, and 45 ± 13(at 1 Hz) to 2,069 ± 198(at 18 Hz) for the SHL group, respectively. Figure 5 displays the

Table 4 Mean of estimated Qc values with the standard error at different central frequencies, for each lapse time, computed for all different stations

Frequency (Hz)	Qc							
	20 s	30 s	40 s	50 s	60 s	70 s	80 s	90 s
Measures of Qc, averaged all over the stations for AR group, for different lapse time and frequency								
1.0	32 ± 11	50 ± 12	84 ± 16	110 ± 20	135 ± 22	134 ± 19	144 ± 25	218 ± 33
1.5	68 ± 13	91 ± 15	136 ± 25	170 ± 27	235 ± 36	207 ± 38	228 ± 34	372 ± 55
2.0	122 ± 26	136 ± 27	192 ± 30	227 ± 50	365 ± 64	292 ± 48	312 ± 50	450 ± 76
3.0	257 ± 28	279 ± 29	428 ± 45	514 ± 80	607 ± 95	542 ± 80	562 ± 79	865 ± 165
4.0	326 ± 30	376 ± 35	569 ± 71	650 ± 96	861 ± 100	750 ± 94	920 ± 83	1,337 ± 271
6.0	474 ± 49	547 ± 45	807 ± 83	918 ± 102	1,220 ± 142	1,110 ± 131	1,280 ± 137	1,640 ± 290
8.0	607 ± 55	755 ± 80	1,063 ± 126	1,300 ± 150	1,489 ± 165	1,490 ± 166	1,800 ± 168	2,360 ± 302
12.0	1,000 ± 105	1,240 ± 110	1,655 ± 139	1,960 ± 185	2,020 ± 201	2,050 ± 206	2,600 ± 202	3,040 ± 333
16.0	1,390 ± 150	1,803 ± 135	2,266 ± 165	2,550 ± 201	2,793 ± 255	3,000 ± 276	3,520 ± 280	3,928 ± 377
18.0	1,525 ± 166	2,078 ± 211	2,567 ± 250	3,240 ± 265	3,278 ± 270	3,945 ± 300	4,200 ± 364	5,150 ± 400
Measures of Qc, averaged all over the stations for SHL group, for different lapse time and frequency								
1.0	23 ± 10	45 ± 13	76 ± 15	62 ± 18	85 ± 20	95 ± 22	113 ± 24	200 ± 36
1.5	48 ± 14	78 ± 16	132 ± 28	141 ± 26	176 ± 29	178 ± 31	215 ± 37	360 ± 59
2.0	72 ± 18	129 ± 23	190 ± 30	196 ± 32	253 ± 49	278 ± 51	349 ± 57	480 ± 76
3.0	198 ± 21	305 ± 31	409 ± 41	406 ± 43	487 ± 75	513 ± 81	637 ± 82	704 ± 103
4.0	268 ± 27	397 ± 47	570 ± 76	543 ± 78	643 ± 93	620 ± 89	762 ± 95	990 ± 110
6.0	440 ± 40	583 ± 64	827 ± 87	718 ± 100	825 ± 98	786 ± 106	943 ± 176	1,230 ± 122
8.0	683 ± 57	881 ± 100	1,096 ± 107	1,027 ± 110	1,087 ± 111	1,300 ± 155	1,430 ± 190	1,890 ± 210
12.0	1,093 ± 110	1,370 ± 122	1,673 ± 170	1,623 ± 198	1,729 ± 161	2,040 ± 189	2,220 ± 225	2,760 ± 287
16.0	1,454 ± 155	1,832 ± 140	2,342 ± 220	2,176 ± 221	2,372 ± 280	2,660 ± 299	3,100 ± 240	3,880 ± 301
18.0	1,650 ± 169	2,069 ± 198	2,749 ± 261	2,496 ± 265	2,734 ± 305	3,370 ± 334	4,260 ± 348	4,800 ± 398
Measures of Qc, averaged all over the stations for IBR group, for different lapse time and frequency								
1.0	22 ± 8	49 ± 14	78 ± 16	86 ± 21	93 ± 25	117 ± 27	137 ± 30	180 ± 37
1.5	42 ± 12	84 ± 26	120 ± 28	144 ± 27	175 ± 30	202 ± 35	223 ± 38	330 ± 42
2.0	59 ± 18	110 ± 28	169 ± 30	228 ± 45	291 ± 48	308 ± 50	347 ± 55	560 ± 64
3.0	142 ± 27	244 ± 31	391 ± 49	541 ± 56	658 ± 84	638 ± 96	785 ± 102	1,045 ± 88
4.0	212 ± 33	346 ± 39	533 ± 66	767 ± 97	868 ± 97	921 ± 99	1,155 ± 135	1,360 ± 97
6.0	356 ± 60	545 ± 52	771 ± 84	1,129 ± 121	1,290 ± 130	1,182 ± 125	1,450 ± 140	2,250 ± 144
8.0	541 ± 76	778 ± 98	1,073 ± 113	1,566 ± 127	1,814 ± 158	1,780 ± 177	2,300 ± 173	3,600 ± 287
12.0	912 ± 109	1,400 ± 105	1,777 ± 167	2,619 ± 250	3,171 ± 270	3,040 ± 288	3,460 ± 195	4,660 ± 303
16.0	1,309 ± 182	2,154 ± 150	2,573 ± 279	3,688 ± 296	4,000 ± 300	3,940 ± 307	4,400 ± 218	5,940 ± 386
18.0	1,602 ± 204	2,466 ± 197	3,136 ± 290	4,401 ± 308	4,990 ± 355	5,120 ± 494	5,740 ± 378	7,460 ± 402

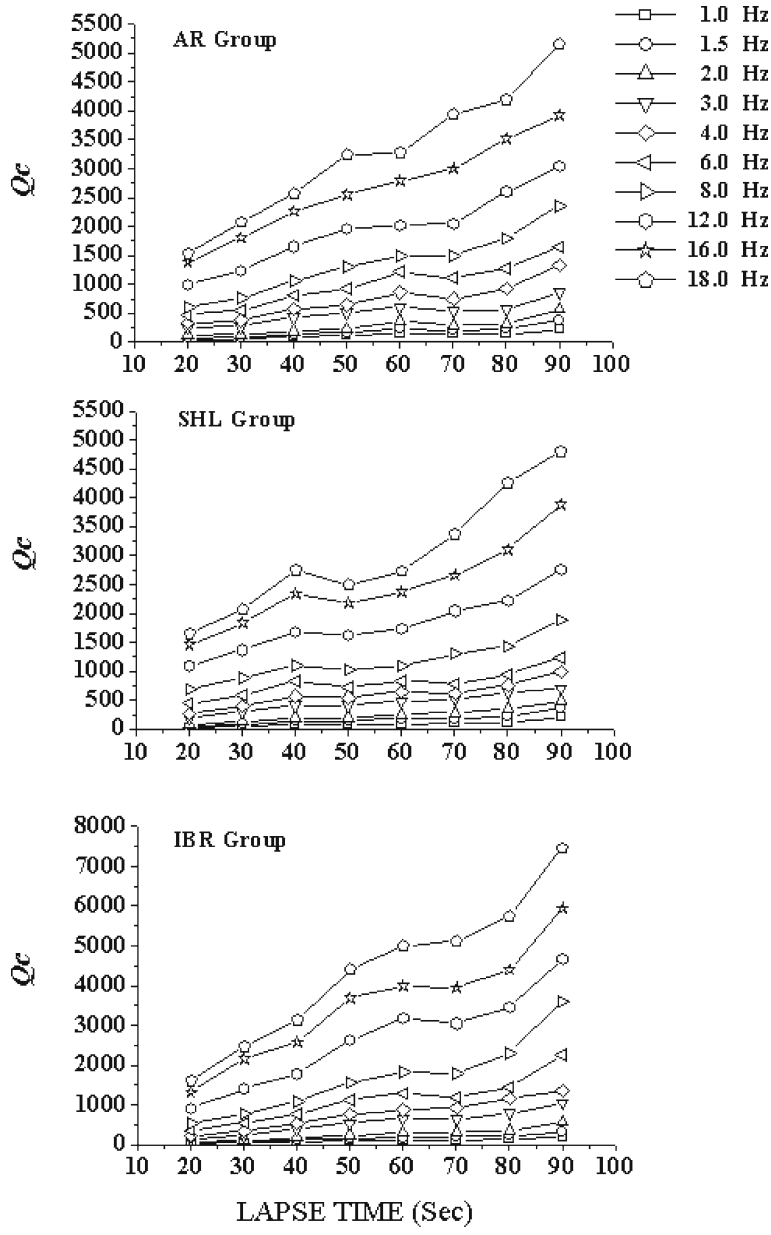

Fig. 6 Variation of average Qc values in AR, SHL, and IBR groups with increasing lapse time coda windows for the selected ten frequency bands (1–18 Hz)

average coda Qc values plotted as a function of frequency for 30-s lapse time window. All the stations show almost similar variation of average Qc with frequency despite the fact that the ray paths for events in each group interact diverse volume of the earth's crust. In addition, at low frequency band, the Qc values vary marginally with frequency at all the stations in all three blocks. Significantly, the TZR station, in the SHL block, however, shows low Qc value at lower-frequency range (Fig. 5). Further, the analysis yields frequency dependence of Qc incidentally allow us to make a regression analysis for each earthquake group, assuming a power law of the form $Qc\ (f) = Qo(f/fo)^n$, where fo = 1 Hz, Qo is the value of Qc at 1 Hz called attenuation parameter and n is the degree of frequency dependence (Aki 1980). Qo and n represent the level of heterogeneity and tectonic activity in the region (Mukhopadhyay and Tyagi 2007). The regression analysis results $Qo = 57.321 \pm 1.07$ and $n = 1.256 \pm 0.034$ for events located in the AR

group. Similarly, $Qo = 48.574 \pm 1.04$ and $n = 1.36 \pm 0.023$ are determined for the IBR group of events while SHL group of events corresponds to $Qo = 53.156 \pm 1.10$ and $n = 1.315 \pm 0.054$. The empirical attenuation relations for all the groups are shown in the top of Fig. 5 whereas attenuation relation particularly obtained for TZR station is shown in the bottom for each group. Comparatively low Qo value estimated at TZR station in each group indicate that the structure beneath TZR station is more heterogeneous compared to other station. To summarize, averaging all Qc values irrespective of tectonic block, we obtain the attenuation relation for the entire NER India as $Qc = 52.315 \pm 1.07\, f^{(1.32 \pm 0.036)}$.

Finally, all the seismograms are analyzed at different lapse time windows, as mentioned earlier, to study the effect of increasing time window on the estimation of Qc values for each group. Figure 6 shows the variation of average Qc with increasing lapse time window considering all frequencies. It is clear from Fig. 6 that Qc values in each group is lapse time dependent and increases with increase in lapse time seem to be in agreement with Del Pezzo et al. (1990). Moreover, Qc values estimated from different lapse time windows are found to be increasing with increase in frequency. For the SHL group, at 40-s lapse time window, there is a distinctive rise in average Qc values at the frequency bands from 4 to 18 Hz. Marginal rise in average Qc is observed for the IBR group of events for the lapse time range 50 to 70 s at the frequency bands 6 to 18 Hz. Moreover, the value of Qo (i.e., Qc at 1 Hz) increases with increase in lapse time window. The distribution of Qc observations, made for each lapse time window, is represented in Fig. 7 and plots of these values as a function of frequency for all three regions are shown in Fig. 8 along with attenuation relations. The correlation coefficient for each window varies from 0.96 to 0.99. This observation strongly indicates that attenuation at higher frequencies is less pronounced than at lower frequency.

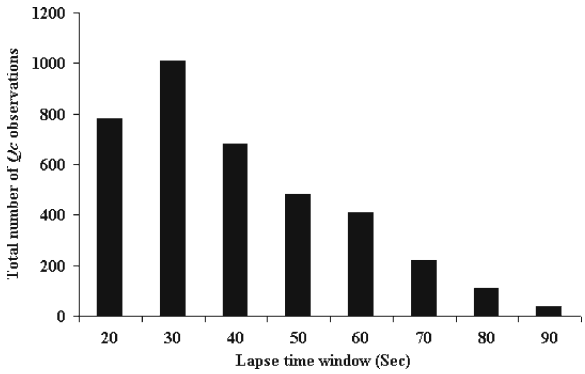

Fig. 7 Distribution of Qc observations made for eight different coda window lengths

5.2 Attenuation parameters

Several authors (e.g., Aki 1980; Pulli and Aki 1981; Roecker et al. 1982; Van Eck 1988; Akinci et al. 1994; Hellweg et al. 1995; Gupta et al. 1998; Biescas et al. 2007) have shown a strong correlation between the degree of frequency dependence and level of tectonic activity for different tectonic regions. They ascertained higher n value for tectonically active regions compared to the stable regions. The value of n is higher at lower lapse time of coda window. The attenuation parameters vary from $Qo = 45.01 \pm 1.13$ and $n = 1.27 \pm 0.069$ at 20 s to $Qo = 185.28 \pm 1.09$ and $n = 1.15 \pm 0.048$ at 90 s for the AR group. For the SHL group, the values are $Qo = 28.73 \pm 1.12$ and $n = 1.46 \pm 0.062$ at 20-s window and $Qo = 114.34 \pm 1.06$ and $n = 1.19 \pm 0.036$ at 70 s. Consequently, for the IBR group of earthquakes, the values are found to be $Qo = 23.87 \pm 1.06$; $n = 1.47 \pm 0.034$ at 20 s and $Qo = 137.32 \pm 1.14$; $n = 1.25 \pm 0.056$ at 70 s. A significant result of this study shows inconsistent Qo values among these three regions which indicate the level in tectonic activity and heterogeneity.

5.3 Sampled area and comparison of Qc^{-1}

According to Pulli (1984), the Qc estimates reflect the average attenuation properties of a volume covered by coda waves, which may be considered as an ellipsoid. For a given lapse time t, the surface projection of this ellipsoid for a surface source can be written as

$$\frac{x^2}{(vt/2)^2} + \frac{y^2}{\left[(vt/2)^2 - R^2/4\right]} = 1$$

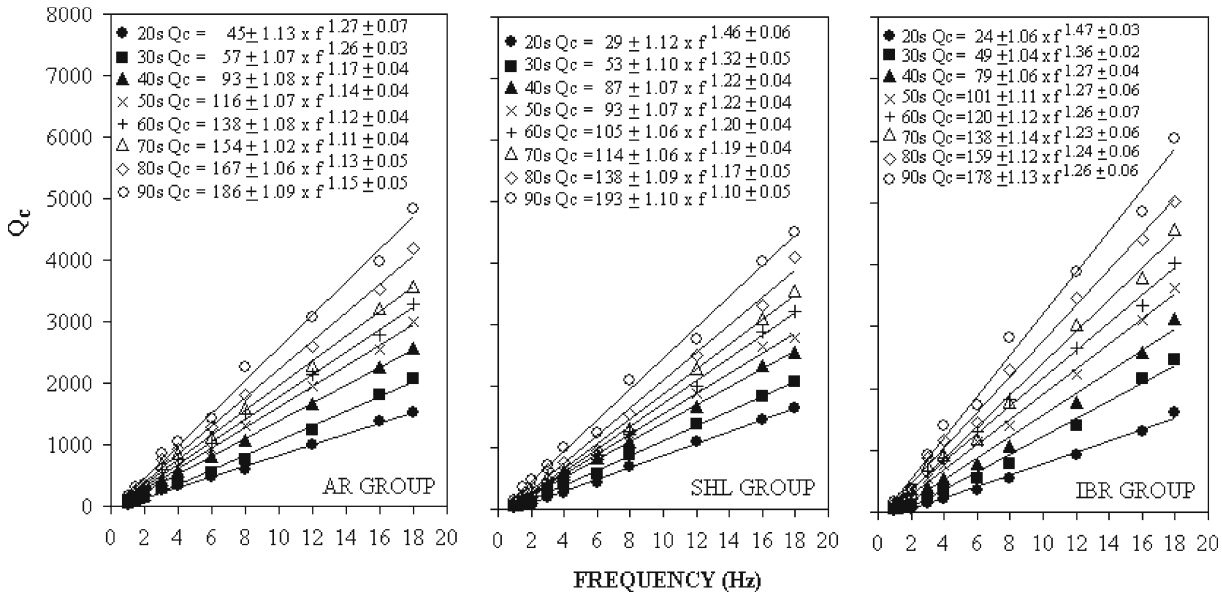

Fig. 8 Comparison of mean of Qc as a function of frequency obtained at eight different coda window lengths for AR, SHL, and IBR group of events

where R is the source-to-station distance, v is the S-wave velocity (3.5 km/s) and x and y is the surface coordinates. In this study, the longest event–station distance 217 km for the AR region, 228 km for the SHL, and 270 km for the IBR are considered to calculate the surface area projection for lapse time window of 70, 80, and 90 s. Sometimes, for lapse time greater than 90 s, the duration of the event ceases and in some cases the signal-to-noise ratio becomes extremely lower. In rationale as in Fig. 3, for the AR group, the coda wave would sample a surface area of 21,874 km^2 inside a spherical shell. Likewise, the coda wave would sample a surface area of 35,742 km^2 and 40,088 km^2 for

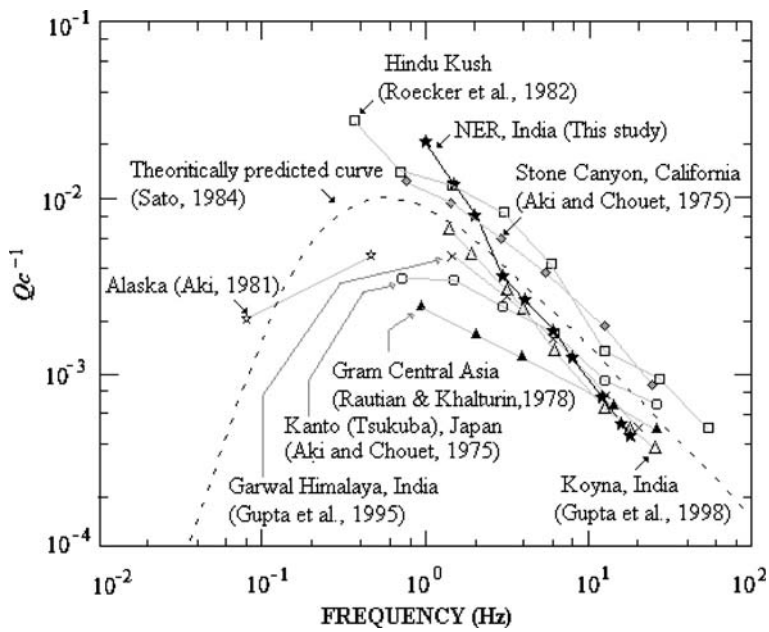

Fig. 9 A comparison of Qc^{-1} as a function of frequency obtained for North Eastern Region of India with the Qc^{-1} observations of other tectonic regions in the world

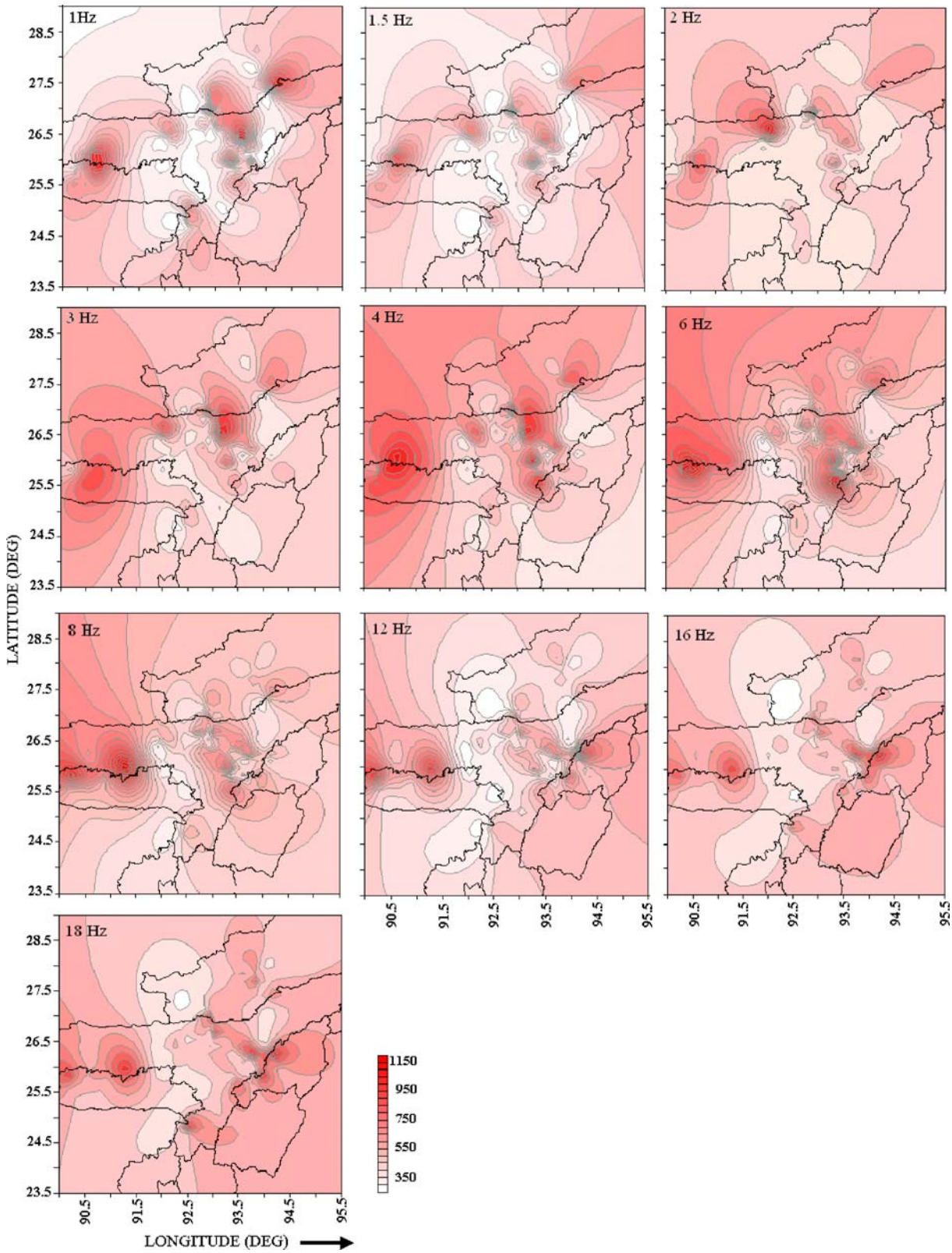
1Hz
1.5 Hz
2 Hz
3 Hz
4 Hz
6 Hz
8 Hz
12 Hz
16 Hz
18 Hz
LATITUDE (DEG)
LONGITUDE (DEG)
28.5
27.5
26.5
25.5
24.5
23.5
90.5
91.5
92.5
93.5
94.5
95.5
1150
950
750
550
350

◀ **Fig. 10** Contour map depicting spatial variation of Qc values at ten central frequencies for 30-s coda window. It is noted that higher attenuations are observed at active tectonic blocks

the SHL and IBR groups, respectively. While estimating the radius of the sphere to be sampled by the coda wave, there is an overlapping volume among these three surface areas. Further to the analysis, a comparison of Qc^{-1}, estimated from the analysis of 30-s lapse time window, as a function of frequency has been made for NER India (as shown in Fig. 9) with Qc^{-1} observations for other tectonically active region of the world, e.g., Hindukush (Roecker et al. 1982), Alaska (Aki 1981), Garhwal Himalaya (Gupta et al. 1995), Stone Canyon (Aki and Chouet 1975), Koyna India (Gupta et al. 1998), etc. It is observed that the NER shows an intermediate trend comparable with the global trend and with the theoretically predicted curve of Sato (1984). It is observed that Qc^{-1} is about $10^{-1.8}$ at 1 Hz and decreases to about $10^{-3.6}$ at 18 Hz. The frequency dependence within the region can be written as $Qc^{-1} \alpha f^{-n}$ for $f > 1$ Hz, where $n \sim 0.5$–1.0. The fact that decay pattern of Qc^{-1} values in the frequency range (1–3 Hz) shows much higher frequency dependence compared to other tectonically active regions like Hindukush, Garhwal Himalaya, and Koyna, India etc.

5.4 Qc map

Three thousand eight hundred ninety Qc values so calculated in each station for every earthquake event in the three tectonic blocks are used for a spatial distribution map of the attenuation factor. Towards the preparation of this map, a few values are interpolated through Krigging method. In order to portray the spatial distribution map, Qc values assigned to the midpoint of epicenter–station trajectories are considered. Figure hyperlinkfig1110 shows the spatial distribution of Qc which corresponds to 30-s lapse time window at all the ten frequency bands. The plot indicates higher Qc values in parts of AR and SHL blocks compared to the IBR block at 1–8 Hz. On the other hand, the Qc values are found to be increasing for the IBR between the range 12–18 Hz. In-depth observation indicate that western part of the AR near Bomdila, eastern part of the SHL, and parts of upper Assam valley near Jorhat represent higher attenuation at all the frequencies. Simultaneously, Mikir hills and western part of Shillong plateau are characterized by lower attenuation, best outlined at 6 Hz (Fig. 10). The contour map obtained corresponds to several high Qc and low Qc areas in this region. In other words, our results suggest that the Qc is lower in areas where the basement depth is deeper and higher where it is shallower.

6 Discussion

The seismic attenuation of northeastern India had never been studied in detail. In the present study, coda Q has been measured for AR, SHL, and IBR group of events of NER India using single scattering model. We have utilized single backscattering model since it gives a reasonably good approximation to our data. It is because we have used microearthquake data (magnitude ~1.2 to 3.9) whose energy is very weak and consequently the scattered wave energy is also too weak. In general, the average value of Qc shows dependence on both lapse time and frequency (Table 3). However, the most remarkable result of our study is that the Qc values are found to be highly frequency dependent at each lapse time window in each tectonic block of NER India. The variation of Qc is 97% (from 50 ± 12 to $2{,}078 \pm 211$) and 96% (144 ± 25 to $4{,}200 \pm 364$) at lapse time window of 30 and 80 s, respectively. Almost similar trend is observed for other lapse time windows. This can be attributed to the active tectonics where the crust is highly heterogeneous. Average attenuation relation $Qc = 52.315 \pm 1.07 f^{(1.32 \pm 0.036)}$ shows that the attenuation is highly dependent on the frequency which is in agreement with the high tectonic activity of northeastern India. The values of Qc measured particularly at TZR station is found to be very low compared to other station data. The average attenuation relations observed from Qc values of all the seismic stations (as given in top of Fig. 5) and the relationship obtained at TZR station (as

in bottom of Fig. 5) shows that Qo value at TZR is almost 50% less compared to average Qo value obtained from all the stations. However, high frequency dependence is reflected in all the attenuation relations. The low value of Qc at TZR station indicates a more heterogeneous structure beneath the TZR station. The calculation of Qc functions gives an idea of spatial variation of attenuation among the three tectonic blocks and can be attributed to geological characteristics of the block. This may indicate that the structure of the upper part of the crust is much more heterogeneous than the deeper part of crust. It is known that Shillong–Mikir plateau is characterized by oceanic crust composed of deposition by heavy high-density minerals while the other two blocks which are a part of continental crust composed of low-density material. As we know, loss of energy is less in high-density material, so the oceanic crust has lower attenuation than continental crust. Hence, most of the Shillong–Mikir hills are characterized by lower attenuation while Arunachal Himalaya and Indo-Burmese region are characterized by higher attenuation. Our result as observed in Qc map agree with this argument. In general, Qc values even at similar epicentral distance indicate some dependency with focal depth. But this is not always true. Our study find that compatible Qc are estimated for a shallow event depth $h = 10$ km, $M_D = 2.7$, $\Delta = 64$ km (Ev. No. 8) and for deeper event $h = 35$ km, $M_D = 2.7$, $\Delta = 58$ km (Ev. No. 5) with equivalent epicentral distances at the same recording station (DMK) in all frequency bands. The Qc values indicate negligible focal depth dependence which does not extend to a large epicentral distance beyond 70 km as a function of lapse time. It implies that the behavior could be due to more or less homogeneous medium in shorter epicentral distance although some studies suggest that velocity contrast in a layered structure produce differences in the Qc (Hoshiba 1997; Margerin et al. 1998).

Simultaneously, when we compare the attenuation parameters among three tectonic groups, Qo value for IBR group is the lowest (Fig. 8). Basically, this estimate is the average estimate of various stations at the respective group. The lower Qo value at IBR group indicates the probable region for occurrence of large earthquakes as observed for the Tangsheng region by Jin and Aki (1986). The lower Qo value may also indicate the presence of lateral heterogeneities in the structure. Present seismicity rate shows that IBR region is tectonically very active compared to the other two regions. The relatively low Qo value reflects the strong scattering effects of the highly dense faulted structure in the region. The degree of frequency dependence n is a little bit higher for TZR station in AR, SHL, and IBR groups which is in agreement with dense fracturing and crisscrossing of faults and lineaments that characterize the particular site. If the standard deviation of Qo is considered, there are no major differences from one region to another. However, if we look at results of individual Qo value of IBR and SHL group, the distinction between higher Qo values for SHL and lower Qo values indicate that the Naga–Disang fault is a kind of boundary between two different attenuation zones. Thus, the northern part of Naga–Disang fault has less attenuation than the southern part of the fault.

Looking at the comparison of Qc^{-1} measurements with other regions for the similar lapse time and frequency range, we observe that NER acquires an intermediate trend among other tectonically active regions of the world and, therefore, the studied parameters show a good consistency.

Qc is an important parameter for comparison of different tectonic regions of the world. However, complexity of the region can be well inferred through estimation of scattering and intrinsic attenuation and their relative contribution towards the total attenuation quality factor of coda wave, which is a scope for further study.

7 Conclusion

In the present study, the Qc values have been estimated for the NER of India using the single scattering model. The coda waves of 187 seismograms from 45 local earthquakes recorded digitally in the NER are analyzed for eight different lapse time window durations (e.g., 20, 30, 40, 50, 60, 70, 80, and 90 s) at ten frequency bands with a central frequency in the range of 1.0 to 18 Hz. The epicentral distance and focal depths of these

events vary from 16 to 270 km and from 7 to 38 km, respectively, having the magnitude less than 4.0.

The mean Qc for 30-s lapse time window varies from 50 ± 12 (at 1 Hz) to 2,078 ± 211(at 18 Hz) in AR, from 49 ± 14 (at 1 Hz) to 2,466 ± 197 (at 18 Hz) in IBR, and from 45 ± 13 (at 1 Hz) to 2,069 ± 198 (at 18 Hz) in SHL. The study indicates that Qc is a function of frequency. A frequency-dependent relationship for the AR is $Qc = 57.321 \pm 1.07\ f^{(1.256\pm0.034)}$, for the IBR $Qc = 48.574 \pm 1.04\, f^{(1.36\pm0.023)}$, and for the SHL $Qc = 53.156 \pm 1.10\ f^{(1.315\pm0.054)}$. An average attenuation relation $Qc = 52.315 \pm 1.07\, f^{(1.32\pm0.036)}$ portrays the average attenuation relation for northeastern India. The average Qc values at each station for the three tectonic blocks show that at low-frequency band they vary marginally. Except for a strong local site effect at the station TZR, the Qc at the other stations is fairly similar, even though the coda waves sample slightly different volumes. Low Qc values estimated at the TZR station may be due to difference in structure that exists beneath this station.

Towards the estimation of Qc, the effect of increasing frequency bands is observed. At higher-frequency bands, the Qc values increase moderately while marginal increments are observed at lower-frequency bands.

An analysis of coda waves at eight different lapse time windows indicates that Qc is lapse time dependent in the region. The Qc values increases as lapse time window increases (Fig. 8). The value of degree of frequency dependence n is found to be higher at lower lapse time. The decrease in the value of n for longer lapse time window for each of the three tectonic blocks indicates a strong correlation with tectonic activity. The attenuation at higher frequencies is less pronounced than at lower frequency. The frequency-dependent average attenuation parameter for the IBR is found to be lowest. The lowest Qo value at IBR indicates the probable region for occurrence of large earthquake. The low Qo value reflects the strong scattering effects of the highly dense faulted structure in the region. The study also indicates that the Naga–Disang fault is a kind of boundary between two different attenuation zones and the northern part of Naga–Disang fault has less attenuation than the southern part of the fault.

The patterns of Qc^{-1} with frequency are analogous to the estimates obtained in other tectonic areas in the world, except with the observation that the Qc^{-1} is much higher at 1 Hz for the study region. The Qc^{-1} is about $10^{-1.8}$ at 1 Hz and decreases to about $10^{-3.6}$ at 18 Hz indicating clear frequency dependence.

Attenuation pattern shows that the western part of the Arunachal Himalaya near Bomdila, eastern part of the Shillong Plateau, and parts of upper Assam valley near Jorhat represent higher attenuation at all the frequencies. The Mikir hills, Arunachal Himalaya, and western part of the Shillong plateau are characterized by lower attenuation best outlined at 6 Hz.

Acknowledgements The author (SB) thank Dr. P. G. Rao, Director, RRL, Jorhat for giving permission to publish the work and render special thanks to Prof. H. K. Gupta, Rammana Fellow, NGRI-Hyderabad, for necessary suggestion to improve the quality of the work and Dr. B. K. Bansal, Director, DST, New Delhi for his kind support to the project. Many thanks are due to Prof. S. S. Arifiev, Schmidt United Institute of Physics of the Earth, Moscow for helping in deriving the response and noise curve of the seismic stations. We are thankful to Dr. J. R. Kayal, Geological Survey of India, Kolkata and Prof. H. Sato, Tohuku Univerity and Dr. S. C. Gupta, IIT-Roorkee, for their critical comments towards the enhancement of the project. Constructive comments from two anonymous reviewers have helped us to improve the paper. The DST provides financial supports for this work vide reference no. DST/23(229)/ESS/2000.

References

Aki K (1969) Analysis of the seismic coda of local earthquakes as scattered waves. J Geophys Res 74:615–631

Aki K (1980) Attenuation of shear-waves in the lithosphere for frequencies from 0.05 to 25 Hz. Phys Earth Planet Inter 21:50–60

Aki K (1981) Source and scattering effects on the spectra of small local earthquakes. Bull Seismol Soc Am 71:1687–1700

Aki K, Chouet B (1975) Origin of coda waves: source, attenuation, and scattering effects. J Geophys Res 75:3322–3342

Akinci A, Taktak AG, Ergintav S (1994) Attenuation of coda waves in Western Anatolia. Phys Earth Planet Inter 87:55–165

Baruah S (2001) Attenuation of coda waves of few local events in NER, India. In: International conference on

seismic hazard with particular reference to Bhuj earthquake of January 26, 2001, vol 1, pp 261–262
Baruah S (2004) Interim progress report submitted to Department of Science and Technology DST, New Delhi, vol 2, pp 1–10
Baruah S, Duarah R, Yadav DK (1997) Pattern of seismicity in Shillong Mikir plateau and the orientation of principal compressive axis. J Geol Soc Ind 49:533–538
Biescas B, Rivera J, Zapata AJ (2007) Seismic attenuation of coda waves in the eastern region of Cuba. Tectonophysics 429:99–109
Bilham R, England P (2001) Plateau pop-up during the 1897 Assam earthquake. Nature 410:806–809
BMTPC (2003) Vulnerability atlas—2nd edn; peer group MoH & UPA; seismic zones of India IS: 1983–2002, BIS, GOI, Seismotectonic atlas of India and its environs, GSI, GOI
Chen WP, Molnar P (1990) Source parameters of earthquakes and intraplate deformation beneath the Shillong Plateau and the Northern Indoburman ranges. J Geophys Res 95:12527–12552
Curray JR, Emmel FJ, Moore DG, Raitt RW (1982) Structure, tectonics, and geological history of the northeastern Indian Ocean. In: Nairu AEM, Stehli FG (eds) The ocean basins and margins, vol 6. Plenum, New York, pp 399–450
Del Pezzo E, Allotta R, Patane D (1990) Dependence of Qc(coda-Q) on coda duration time interval: model or depth effect? Bull Seism Soc Am 80:1028–1033
Fitch TJ (1970) Earthquake mechanism in the Himalayan, Burmese and Andaman regions and continental tectonics in Central Asia. J Geophys Res 75:2699–2709
Gao LS, Lee LC, Biswas NN, Aki K (1983) Comparison of the effects between single and multiple scattering on coda waves for local earthquakes. Bull Seismol Soc Am 73:377–389
Giampiccolo E, Gresta S, Rascona F (2004) Intrinsic and scattering attenuation from observed seismic codas in Southeastern Sicily (Italy). Phys Earth Planet Inter 145:55–66
Gupta HK, Singh HN (1986) Seismicity of the North-East India region, part II: earthquake swarms precursory to moderate magnitude to great earthquake. J Geol Soc Ind 28:367–406
Gupta SC, Kumar A (2002) Seismic wave attenuation characteristics of three Indian regions: a comparative study. Curr Sci 82:407–413
Gupta HK, Singh SC, Dutta TK, Saikia MM (1984) Recent investigations of North East India seismicity. In: Gongxu G, Xing-Yuan M (eds) Proc. international. symp. continental seismicity and earthquake prediction. Seismological Press, Beijing, pp 63–71
Gupta SC, Singh VN, Kumar A (1995) Attenuation of coda waves in the Garhwal Himalaya, India. Phys Earth Planet Inter 87:247–253
Gupta SC, Teotia SS, Rai SS, Gautom N (1998) Coda Q estimates in the Koyna Region, India. Pure Appl Geophys 153:713–731
Hellweg M, Spudich P, Fletcher JB, Baker LM (1995) Stability of coda Q in the region of Parkfield, California: view from the U.S. geological survey parkfield dense seismograph array. J Geophys Res 100:2089–2102
Herak M (1991) Lapse-time dependence Qc-spectra observed in the Dinarides region (Yugoslavia). Phys Earth Planet Inter 67:303–312
Herrmann RB (1980) Q estimates using the coda of local earthquakes. Bull Seismol Soc Am 70:447–468
Hoshiba M (1997) Seismic coda wave envelope in depth dependent S wave velocity structure. Phys Earth Planet Inter 104:15–22
Ibanez JM, Pezzo ED, De Miguel F, Herraiz M, Alguacil G, Morales J (1990) Depth-dependent seismic attenuation in the Granada Zone (Southern Spain). Bull Seismol Soc Am 80:1232–1244
Jin A, Aki K (1986) Temporal change in coda Q before the Tangshen earthquake of 1976 and the Haicheng earthquake of 1975. J Geophys Res 91:665–673
Kayal JR (1996) Earthquake source process in Northeast India: a review. J Himalayan Geol 17:63–69
Khattri KN (1987) Great earthquakes, seismicity gaps and potential for earthquake disaster along the Himalayan plate boundary. Tectonophysics 138:79–92
Le Dain AY, Tapponnier P, Molnar P (1984) Active faulting and tectonics of Burma and surrounding regions. J Geophy Res 89:453–472
Lienert BR, Berg BE, Frazer LN (1986) Hypocenter: an earthquake location method using centered, scaled and adaptively damped least squares. Bull Seismol Soc Am 76:771–783
Margerin L, Campillo M, Tiggelen BV (1998) Radiative transfer and diffusion of waves in a layered medium: new insight into coda Q. Geophys J Int 134:247–258
Mazumder SK (1976) A summary of the Precambrian geology of Khasi Hills, Meghalaya. Misc Publ Geol Surv Ind 23:311–334
Mitchel AHG (1986) Ophiolits and associated rocks in four settings: relationship to subduction and collision. Tectonophysics 125:251–269
Mukhopadhyay S, Tyagi C (2007) Lapse time and frequency—dependent attenuation characteristics of coda waves in Northwestern Himalayas. J Seismol 11(2):149–158(10) April
Nandy DR (2001) Geodynamics of Northeastern India and the adjoining region. ABC Publications, Calcutta, pp 209
Nandy DR, Das Gupta S (1991) Seismotectonics domains of Northeastern India and adjacent areas: geology and geodynamics of Himalayan collision zone, pt. 2: physics and chemistry of earth, no. 1–11, vol 18. Pergamon Press, PLC., Oxford, pp 371–384
Novelo-Casanova DA, Lee WHK (1991) Comparison of techniques that use the single scattering model to compute the quality factor Q from coda waves. Pure Appl Geophys 135:77–89
Okada H, Suzuki S, Asano S (1970) Anomalous underground structure in the Matsushiro earthquake swarm area as derived from a fan shooting technique. Bull Earthq Res Inst Tokyo Univ 48:811–833
Oldham RD (1899) Report of the great earthquake of 12th June 1897. Mem Geol Surv Ind 29:1–379

Peterson J (1993) Observation and modeling of seismic background noise. US Geol Surv Tech Rept 93: 1–95

Poddar MC (1950) The Assam earthquake of 15th August 1950. Indian Minerals 4:167–176

Pulli JJ (1984) Attenuation of coda waves in New England. Bull Seismol Soc Am 74:1149–1166

Pulli JJ, Aki K (1981) Attenuation of seismic waves in the lithosphere: comparison of active and stable areas. In: Beavers JE (ed) Earthquakes and earthquake engineering: the Eastern United States. Ann Arbor Science Publishers Inc., Ann Arbor, pp 129–141

Rautian TG, Khalturin VI (1978) The use of coda for determination of the earthquake source spectrum. Bull Seismol Soc Am 68:923–948

Ravikumar M, Purnachandra Rao N, Chalam SV (1996) A seismotectonic study of the Burma and Andaman arc regions using centroid moment tensor data. Tectonophysics 253:155–165

Richter CF (1958) Elementary seismology. Freeman, San Francisco, pp 768

Roecker SW, Tucker B, King J, Hatzfeld D (1982) Estimation of Q in Central Asia as a function of frequency and depth using the coda of locally recorded earthquakes. Bull Seismol Soc Am 72:129–149

Saikia CK, Somerville PG (1998) Ground motion estimation criteria for large earthquakes in the urban areas of northeast India. J Geophys 19:35–52

Sato H (1977) Energy propagation including scattering effects: single isotropic scattering. J Phys Earth 25: 27–41

Sato H (1984) Attenuation and envelope formation of three-component seismograms of small local earthquakes in randomly inhomogeneous lithosphere. J Geophys Res 89:1221–1241

Satyabala SP (1998) Subduction in the Indo-Burman region. Is it still active? Geophys Res Lett 25:3189–3192

Sitaram MVD, Yadav DK, Goswami K (2001) Study on crustal structure beneath Arunachal Himalaya and Assam. J Geol Soc Ind 58:285–301

Stearns DS, David RA (1988) Signal processing algorithms. Prentice-Hall, Englewood Cliffs, 07632

Tapponier P, Peltzer G, Le Dain AY, Armiju R, Cobbold P (1982) Propagating extrusion tectonics in Asia, New insight from simple experiments with Plasticine. Geology 10:611–616

Tillottson E (1953) The great Assam earthquake of 1950, the completion of papers on the Assam Earthquake of August 15, 1950, Compiled by M.B. Ramchandra Rao, pp 94–96

Van Eck T (1988) Attenuation of coda wave in the Dead Sea Region. Bull Seismol Soc Am 78:770–779

Woodgold CRD (1992) Coda Q in the Charlevoix, Quebec Region dependence on lapse time, comparison to typical eastern Canadian values, and possible long-term change abstract. Eos Trans. AGU, Spring meeting suppl., 200, pp 73–76